JOURNAL OF AIRCRAFT
Vol. 33, No. 5, September–October 1996

Open- and Closed-Loop Results of a Strain-Actuated Active Aeroelastic Wing

Charrissa Y. Lin* and Edward F. Crawley†
Massachusetts Institute of Technology, Cambridge, Massachusetts 02139-4307
and
Jennifer Heeg‡
NASA Langley Research Center, Hampton, Virginia 23681-0001

Open- and closed-loop tests for a strain-actuated active aeroelastic wing are summarized. Linear quadratic Gaussian (LQG) control laws as well as robust control laws are designed using sensitivity weighted LQG, classical rationalization, and multiple models. Significant vibration suppression and load alleviation are demonstrated, reducing the power spectral density of the first mode's response by an order of magnitude. The flutter dynamic pressure is increased by 12%. The three major performance limitations are the saturation limit of the piezoelectrics, the choice of performance metric or output sensor, and the changes in the dynamic response of the test article.

I. Introduction

THE application of aeroelastic control to aircraft offers the promise of smoother rides, larger flight envelopes, and lower root loads, with benefits to life and aircraft size. Numerous investigations have used active control techniques, usually employing articulated trailing-edge control surfaces as actuators.[1-3] The choice of articulated control surfaces is primarily because of the availability of flap actuators on the majority of current aircraft and not their desirability as aeroservoelastic actuators.

The current program seeks to develop and demonstrate a new aeroelastic control actuation method: direct strain actuation. Strain actuators, such as piezoelectrics, provide direct control of the structure with no appreciable lags. The use of flap and aileron actuators for aeroelastic control could impinge upon the primary use of flap and aileron actuators for maneuvering. Strain actuators do not impose any such maneuvering limitations and are not subject to reversal of authority with dynamic pressure. In addition, the easily discretized and distributed nature of piezoelectric actuators provides a flexibility in actuator placement and grouping unavailable with other actuators.

The objective of this work is to demonstrate the use of strain actuation technology for aeroelastic control, specifically flutter suppression and gust alleviation. Significant analytical[4,5] and small-scale experimental work has been done for strain-actuated aeroelastic control. Initial experimental applications have included the use of piezoelectrics as helicopter flap actuators[6] and on the spring support of a rigid two-degree-of-freedom wing model used in flutter suppression.[7] The direct precursor to this experiment was a 1-ft span flat plate with piezoelectrics bonded to the top and bottom surfaces.[8,9]

This article discusses the two wind-tunnel entries of the strain-actuated active aeroelastic wing test program. An initial description of the wing test article is given followed by a brief summary of the open-loop tests conducted during the first wind-tunnel entry. The control design procedure is outlined with a description of the control laws designed. The experimental results of these control laws and those from a midentry redesign are discussed. The final section discusses the factors that limited the performance of the control laws and provides suggestions for future work to alleviate these limitations.

II. Wing Design and Open-Loop Testing

The wing test article was designed to maximize piezoelectric control authority while maintaining the desired passive aeroelastic behavior.[10] A composite sandwich structure, 2% thickness-to-chord ratio, was selected as the primary load-carrying element of the wing. Piezoelectrics are bonded to the top and bottom surfaces and accelerometers and strain gauges are used as sensors. The wing is not dynamically scaled.

An aft geometric sweep of 30 deg was selected as well as a graphite/epoxy (IM7G/3501-6) laminate of $[-20/-20/0]_S$ with reference to the quarter chord line (see Fig. 1). These parameters create a desirable washout configuration that causes

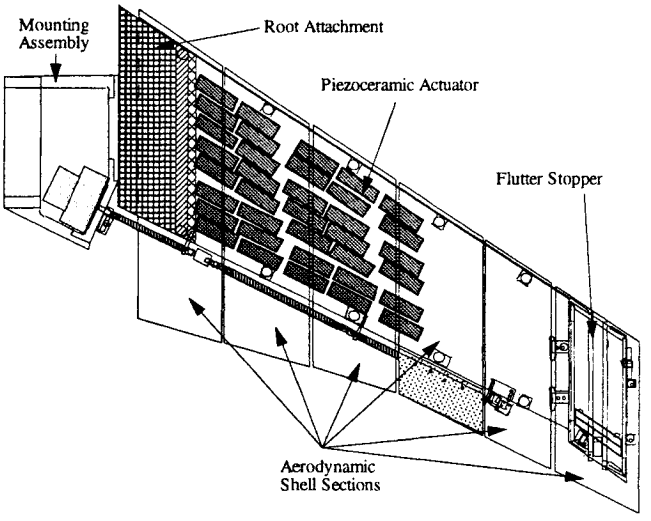

Fig. 1 Schematic of wing.

Presented as Paper 95-1386 at the AIAA/ASME/ASCE/AHS/ASC 36th Structures, Structural Dynamics, and Materials Conference, New Orleans, LA, April 10–12, 1995; received May 28, 1995; revision received April 1, 1996; accepted for publication April 29, 1996.

*Postdoctoral Associate, Department of Aeronautics and Astronautics, Room 37-391, 77 Massachusetts Avenue. Student Member AIAA.

†Professor of Aeronautics and Astronautics and MacVicar Faculty Fellow, Department of Aeronautics and Astronautics, Room 37-351, 77 Massachusetts Avenue. Fellow AIAA.

‡Research Engineer, Aeroelasticity Branch. Member AIAA.

the wing to flutter before it diverges. In addition, both parameters provide bend–twist coupling that enables in-plane isotropic piezoelectric actuators to effect the angle of attack or torsional motion of the wing.

The surface area, thickness, and approximate location of the piezoelectric actuators were selected to maximize the authority for a fixed actuator mass. The piezoelectric actuators are composed of two 10-mil layers of piezoceramic (G-1195) and extend from the root to approximately 60% of the span. The actuators are paired on the top and bottom surfaces and are actuated in a bender configuration. They have been hard-wired into 15 individual actuation groups (see Fig. 2).

A flutter stopper with a spring-loaded moveable tungsten mass was designed to provide a safe condition for the testing of flutter suppression controllers. In the undeployed configuration, the mass is held at the trailing edge by an electromagnet. At the onset of flutter, the mass is deployed to the leading edge. This is known as the deployed configuration. The deployment of the flutter stopper mass alters the wing properties such that the flutter dynamic pressure is increased.

The airfoil selected was a NACA 66-012 made of fiberglass. To ensure that it did not add appreciable stiffness, it was segmented spanwise. Soft rubber tape was used to cover the gaps between the aerodynamic sections. The frequencies of the first three modes for the undeployed configuration at zero airspeed were 2.45, 12.46, and 17.32 Hz, respectively. A more complete description of the wing and modeling can be found in Ref. 11.

The wing test article was tested in air at atmospheric pressure in the NASA Langley Research Center's Transonic Dynamics Tunnel. The objectives of the first wind-tunnel entry were to clear the flutter boundaries of both the undeployed and deployed configurations and to take transfer functions from the piezoelectric groups to the 14 sensors at several dynamic pressures. The transfer functions were taken to support the control design effort, improve finite element models, and estimate the flutter speed more accurately. Based on extrapolation of identified frequencies to the coalescence of the first two modes, the actual flutter dynamic pressures were determined to be 95 and 85 psf for the deployed and undeployed configurations, respectively.

Prototype piezoelectric supergroups were created and tested to examine the authority of a typical actuation group and its signal-to-noise ratio (SNR), as well as potential nonlinearities involved in combining the piezoelectric groups. A total of five groups was created (see Fig. 2), based upon their contributions to the controllability of the first three modes at zero airspeed.

Transfer functions for the individual piezoelectric groups and the piezoelectric supergroups were taken. For a given actuator, transfer functions were taken from input voltage to 14 outputs (see Fig. 3). Turbulence response autospectra, which recorded the sensors' response with no actuation input, were also taken at several dynamic pressures for both configurations. The complete data set is summarized by Heeg et al.[12]

Since combinations of the piezoelectric groups other than the prototype supergroups tested could be desirable for control design, the validity of superposition of the individual piezoelectric transfer functions was examined. The transfer functions for the individual actuators that comprise a supergroup were summed and compared to a supergroup transfer function (see Fig. 4). Although there are nonlinearities associated with the higher modes, the contribution of the individual piezoelectrics to the first three modes superposed linearly. A large portion of the discrepancy is caused by the low coherence of the individual transfer functions. The most likely cause of the nonlinearities was the rubber tape that covered the gaps between aerodynamic sections. This provides stiffness when the

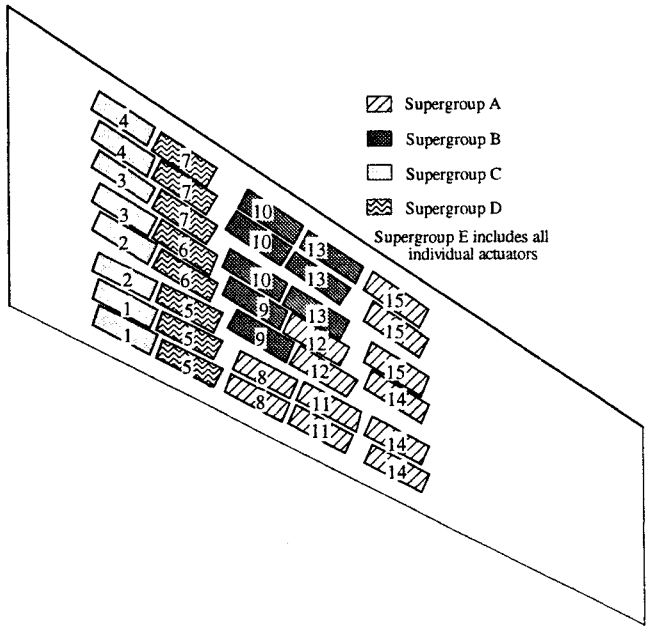

Fig. 2 Schematic of piezoelectric actuation groups and prototype supergroups tested during open-loop testing. Individual piezoelectric groups indicated on diagram. Supergroup 5 includes all 15 individual groups.

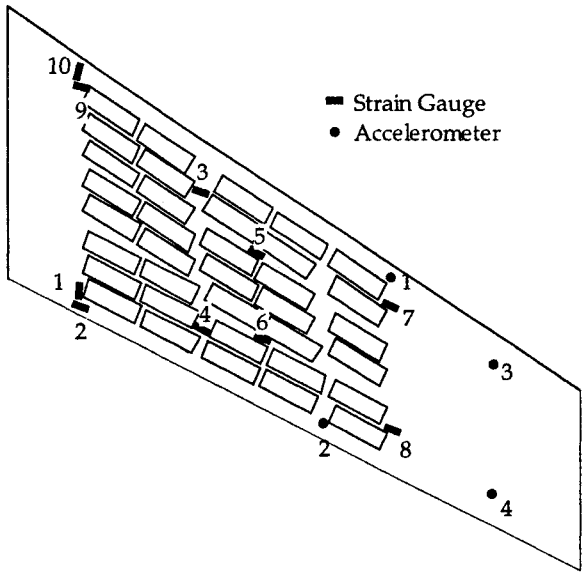

Fig. 3 Location of strain gauges and accelerometers.

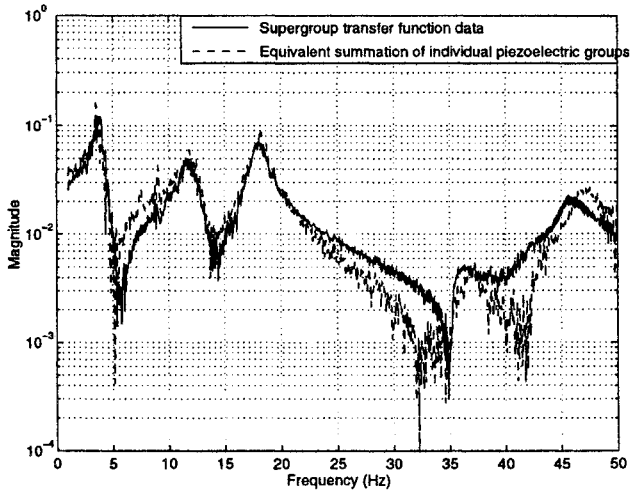

Fig. 4 Comparison of actual supergroup transfer function data to the equivalent summation of individual piezoelectric group transfer function data.

skin is in tension and none when it is in compression. Comparison of these transfer functions provided two warnings to the control designer: 1) to avoid control designs that depend on exact knowledge of the higher modes and 2) to be cautious when using the individual actuator transfer functions to create larger groups. For these reasons, the control laws were designed using the prototype supergroups.

III. Control Law Design and Closed-Loop Testing

A. Control Actuator, Sensor, and Performance Selection

The initial set of control laws was designed based upon the open-loop data taken during the first wind-tunnel entry. The first step in any control design is to specify the performance metric. For aeroelastic control, three objectives are of importance: 1) flutter suppression, 2) ride comfort, and 3) load alleviation. An appropriate performance sensor for flutter suppression is one that has a high response for the flutter mode. Without an accurate model of the flutter mode, the choice is difficult, but may be guided by the modal response in the subcritical data for each sensor. The objective of ride comfort is the acceleration at the passenger location. For a cantilever wing model, a combination of the tip accelerometers or the root strain gauges may be reasonable substitutes. For load alleviation, the root strain gauges can be used to represent the root loading. When the autospectra of the accelerometers' response to turbulence were examined, the modal responses did not rise above the noise floor, except for data taken near flutter. For this reason, the following control designs focus on the root strain as the performance metric. Strain gauges 1 and 2 are used because of their high modal responses.

The next step was to choose the actuator complement. Actuator and sensor choices had to be made to limit the number of topologies considered in control design. As seen from the open-loop testing and transfer functions, individual piezoelectric groups could not provide sufficient authority. In addition, the superposition of individual piezoelectric group transfer functions was suspect for creating new, untested supergroups. The five supergroups tested during the first entry for the control designs were used.

To maximize total actuator authority, the single input/single output (SISO) designs used supergroup E. Because the strain node lines of the higher modes lie within supergroup E, this supergroup can only exert significant authority over the first mode. However, it has been previously shown that a single actuator can only control one mode well, even if it has significant authority over more than one mode.[13] Therefore, choosing supergroup E for the SISO control laws did not limit the overall performance and was likely the best choice, given the first mode's contribution to the overall power spectral density.

The multiple input/multiple output (MIMO) designs used the other four (A–D) supergroups, which together include all 15 individual piezoelectric groups. With four independent actuators, the first four modes could be independently controlled.

The measurement sensor complement was determined through a qualitative examination of the transfer function data. The 70 transfer functions were rated on their level of collocation (i.e., degree of alternating pole/zero pattern), the modal residues or pole/zero spacing, and the SNR of the transfer function data. Those sensors that ranked high in this rating were chosen for the control law designs. Each control law design included at least one of the performance metric sensors.[14] SISO designs used strain gauge 2 (located at the root) as the sensor. MIMO designs used strain gauges 2, 3, 6, and 7 or 1, 2, 6, and 7 as sensors. No accelerometers were used because of the low coherence of their transfer functions, particularly at low frequencies.

Following the selection of actuators and sensors, the dynamics of each of the control loops were identified. The method used for identification employs the frequency domain observability range space extraction (FORSE) algorithm.[15,16] This allows frequency domain data to be automatically fit with a parametric, but nonphysical, state-space model. To further improve the fidelity of the model, a logarithmic tuning step is used. This method allows the control designer to obtain an exceptional fit to the data with a relatively small number of states, even for a MIMO system. Because the measurement model is fitted simultaneously across all of the transfer functions in a MIMO system, a set of poles common to all of the transfer functions is selected. A sample transfer function fit for a four input/four output measurement model identification is shown in Fig. 5.

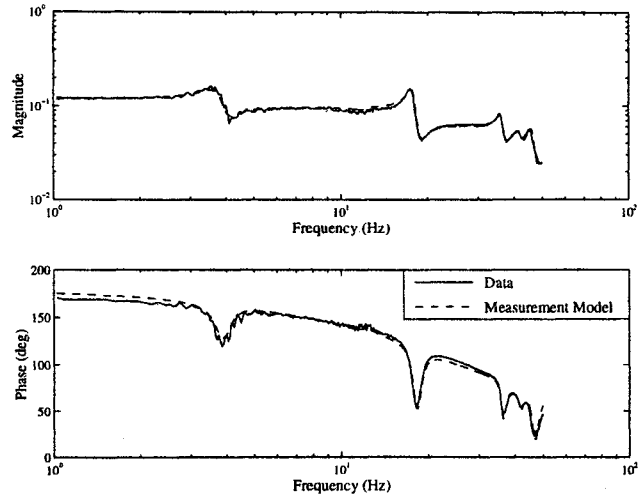

Fig. 5 Comparison of measurement model with transfer function data from supergroup A to strain gauge 6.

B. Initial Control Design

A family of SISO control laws was designed to examine several different robust control methods. The baseline control law was a linear quadratic Gaussian (LQG) design. Three robustified designs included a sensitivity weighted LQG (SWLQG), a classically rationalized, and a multiple model control law. The goal was to gain a better understanding of the properties of the aeroelastic control problem and some of the existing control tools. The nominal design point was chosen to be a dynamic pressure of 50 psf and the control laws that utilized strain gauge 2 as the feedback and performance sensor.

The LQG design methodology is an output feedback scheme that utilizes the linear quadratic regulator (LQR) for a full-state feedback control law and a Kalman filter as the state estimator.[17] The state weighting matrix for LQR is chosen to reflect the weighting of the states in the performance metric and the control weighting matrix is determined by the maximum control. The process noise contribution to the Kalman filter is generally modeled as the effect of the external disturbance on the states. Since the disturbance (wind gust) to sensor transfer functions were not measured during the test and no adequate models existed, the process noise weighting matrix was left as a design parameter. Selection of this matrix can greatly affect the resulting control design and performance. However, no systematic method for choosing an optimal or near-optimal matrix is known. Thus, the selection was based on engineering judgment through an iterative process.

The three robustification techniques are variations on the LQG theme. Sensitivity weighted LQG alters the weighting matrices of both the LQR and Kalman filter portions by adding a sensitivity to parameter variation.[18] In this design, the frequencies of the first two, and sometimes three, modes were weighted. Classical rationalization attempts to mitigate some of the drawbacks of the LQG design technique.[14] Examining an LQG controller, the control designer uses physical intuition and insight to reduce the controller size and remove unnec-

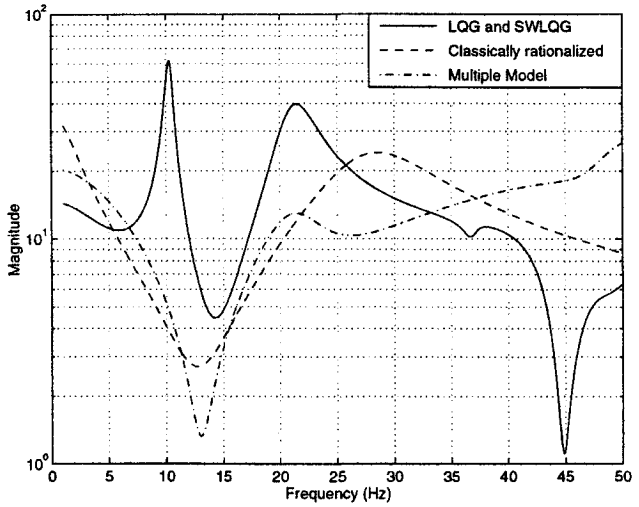

Fig. 6 Comparison of SISO controller transfer functions.

essary and potentially harmful dynamics, such as inverted zeros that appear in the compensator as poles. The multiple model technique minimizes a weighted average of the LQG cost functionals for a discrete set of plants.[18] An added benefit is that the resulting control law will be stable for those particular plants. Drawbacks include the large computational effort required and the need for an initial guess that is stable for all of the plants.

Using these four methods, control laws were designed for the SISO topology using piezoelectric supergroup E (i.e., all of the piezoelectrics) and strain gauge 2 as both the measurement and performance metric at a nominal dynamic pressure of 50 psf. The four controllers that form the full family can be seen in Fig. 6 and Table 1. All of these are stable and roll off before 50 Hz when combined with the plant transfer function. The LQG control law inverts the lightly damped zero between the first and second modes and has many extraneous states. The SWLQG design controller transfer function virtually overlays the LQG design. Very high sensitivity weights were tried with little result. This is because the sensitivity weighting increases the importance of a particular mode in the cost functional. This discourages LQG from notching that particular mode and works well for poorly modeled modes in the crossover region.[14] However, since the modes that were sensitized in this problem are already significant in the cost functional, the sensitivity weighting did not change the compensator transfer function. The classically rationalized design has relatively few states and essentially mimics the LQG design without the inverted zero at 10 Hz and the notch at 45 Hz. The multiple model design used a SWLQG control law designed at a dynamic pressure of 75 psf as an initial guess and the plant at dynamic pressures of 50 and 75 psf as the multiple models. Note that it resembles the classically rationalized design more closely than the LQG or SWLQG designs.

To predict performance, expected closed-loop power spectral densities of the performance sensors were calculated. The calculation required the open-loop power and cross-spectral densities of the performance sensor with only the external disturbance acting, the actuator to sensor transfer function, and the control law. The equations can be seen in the Appendix. The performance improvement is calculated as follows:

$$dB_{\text{Imp}} = 10 \log_{10} \frac{\int_0^{50\,\text{Hz}} \Phi_{z_w z_w}(\omega)\, d\omega}{\int_0^{50\,\text{Hz}} \Phi_{zz}(\omega)\, d\omega} \tag{1}$$

Table 1 Summary of SISO control law designs

Control law	Number of states	Predicted performance at 50 psf	Expected performance at 50 psf
LQG/SWLQG	14	4.26 dB	Unstable
Classically rationalized	4	4.32 dB	2.78 dB
Multiple model	13	3.5 dB	Not tested

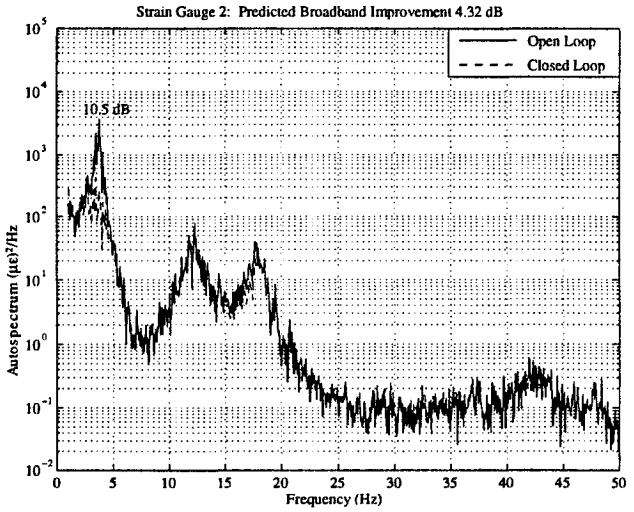

Fig. 7 Open-loop power spectral density and predicted closed-loop power spectral density for classically rationalized control law. Strain gauge 2 is the performance variable.

where $\Phi_{z_w z_w}$ is the open-loop autospectrum of the performance metric and Φ_{zz} is the closed-loop autospectrum.

The open-loop autospectrum and the predicted closed-loop autospectrum for the classically rationalized control law can be seen in Fig. 7. There are several important features to note. The first is that only the first mode is effectively suppressed. This is because the actuation group includes all 15 groups and can only effectively control the first mode, as well as the fact that a single actuator can only effectively control a single mode. The performance of the other control laws is similar. The multiple model does not perform as well at 50 psf because it is also robustified to 75 psf.

The MIMO designs proceeded in a similar manner. A dynamic pressure of 50 psf was used as the nominal design point and LQG was used as the baseline control design technique. In addition to the LQG control laws, SWLQG control laws were designed for the same topologies. Two SWLQG designs were tested: one that used strain gauges 2, 3, 6, and 7 for feedback and one that used strain gauges 1, 2, 6, and 7. For both cases, the four piezoelectric supergroups (A–D) were used and the performance metric consisted of strain gauges 1 and 2.

C. Initial Closed-Loop Testing

Of the SISO control laws, only the SWLQG and the classically rationalized control laws were tested during the second wind-tunnel entry. The first step of the testing procedure for a given control law was open-loop controller performance evaluation at the design point.[19] If the controller were predicted to be stable, the loop would then be physically closed and the dynamic pressure could be slowly increased.

The first control law tested was the SWLQG design. Based upon the open-loop controller performance evaluation, the SWLQG was determined to be unstable at a dynamic pressure of 50 psf. Because of the prediction, the loop was not closed. The predicted instability was traceable to the fairly significant changes in the plant between the first and second wind-tunnel

entries, which are described in greater detail later. The inverted zero in this compensator at 10 Hz (see Fig. 6) caused it to be very sensitive to changes in the frequency of that zero and the frequency of the second mode. Because of its great similarity, it was assumed that the LQG compensator would have been similarly unstable.

The second SISO control law tested was classically rationalized. Because the zero-inversion was eliminated, this design was predicted to be stable and the loop was physically closed. The experimental performance autospectrum can be seen in Fig. 8. The qualitative characteristics match those of the predictions. The spike at 20 Hz was an anomaly in the data-taking mechanisms and not a part of the physical plant.

The first MIMO design, using gauges 2, 3, 6, and 7, was predicted to be unstable based upon the open-loop controller performance evaluation. This compensator failed for reasons similar to the SISO SWLQG compensator: the compensator transfer functions had fairly sharp notches at the second mode. The second MIMO design using gauges 1, 2, 6, and 7 had much smoother behavior over the frequencies near the second mode and was predicted to be stable. The experimental closed-loop performance autospectra can be seen in Fig. 9. As with the SISO control law, these results qualitatively match the prediction very well. Quantitatively, the predicted performance improvement was 4.26 and 5.22 dB for strain gauges 1 and 2, respectively, and the experimental performance improvement was 2.53 and 4.13 dB, respectively.

D. Discussion of Initial Control Design Results

The testing of the initial control designs met several of the overall project objectives. Load alleviation was demonstrated on the model. Both the successful SISO and MIMO control laws were able to reduce vibrations at the root.

The results of the MIMO control law showed that effective modal control of the first three modes, and thus the torsional motion, was obtained. This confirmed that effective torsional control can be obtained using isotropic actuators on a bend–twist coupled laminate. It also showed that the grouping of the piezoelectric actuators is crucial for modal control. In Lazarus' experiment,[9] the piezoelectric actuators were grouped spanwise, even on the graphite/epoxy bend–twist coupled plate. This spanwise grouping was not effective in achieving torsional control.

Furthermore, although both the SISO and MIMO designs accomplished their performance objectives of lowering strain levels at the root, visual observation of wing motion indicated little to no performance improvement. In addition, neither control law was able to alter the flutter speed. Visual observation tends to reflect tip motion, and the performances for the trailing-edge tip accelerometer for the SISO and MIMO control laws were −0.59 and −1.86 dB, respectively. The negative values indicate that the motion was exacerbated at the tip by these two control laws.

This observation led to two conclusions: 1) Damping of the first three modes does not delay the onset of flutter. These two control laws were designed primarily with damping of the first three modes as the primary goal. Therefore, a more appropriate performance metric should be chosen. 2) The root strain gauges may not have been the best sensors to use to quiet the wing as a whole or to move the flutter boundary.

The other difficulty encountered in testing the initial control laws was the substantial changes in the open-loop plant between the two wind-tunnel entries. Most noticeably, the open-loop flutter speeds for both configurations were lowered. The test article fluttered at 76 psf for the undeployed configuration and 86 psf for the deployed configuration during the first entry vs 85 and 95 psf during the second, respectively. Furthermore, the transfer functions at a dynamic pressure of 50 psf, still well below the flutter speed, were significantly altered (see Fig. 10). The most problematic change in the transfer function shown is the frequency of the second mode and the immediately preceding zero. With these values shifted down by approximately 10%, the LQG and SWLQG compensators, which either inverted the zero or placed a notch filter at the pole frequency, experienced stability problems.

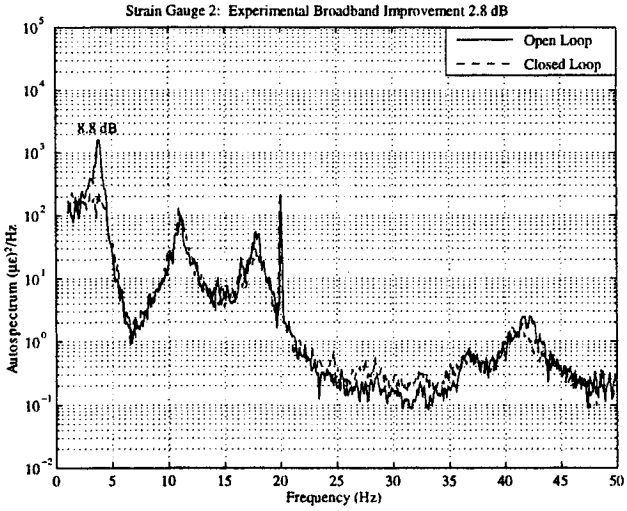

Fig. 8 Experimental open- and closed-loop power spectral densities for classically rationalized control law. Strain gauge 2 is the performance variable.

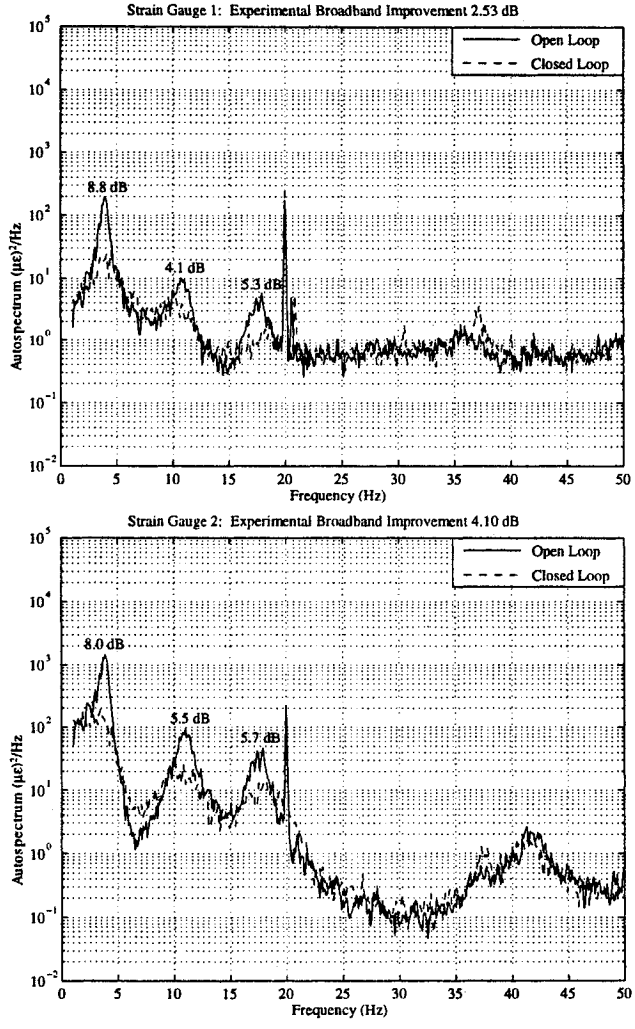

Fig. 9 Experimental open- and closed-loop power spectral densities for MIMO control law. Strain gauges 1 and 2 are the performance variables.

While the changes at speed were marked, the plant at zero airspeed seemed to be relatively unchanged. The frequencies did not alter significantly between the two entries (see Table 2). This leads to the conclusion that the plant changes are caused by the shell attachments and the overall twist of the wing. Through different attachment tightnesses or fatigue over the months, these two factors could have slightly altered the distributed angle of incidence. This would change the aerodynamic behavior without dramatically affecting the structural modes.

E. Controller Redesign

Because of the changes in the plant and the realization that the chosen output feedback sensors and performance metric were suboptimal, a redesign of control laws was completed during the second entry. The open-loop transfer function data taken at the beginning of the second entry were used to identify new state-space models to be used in the redesign. These control laws were tested in lieu of the remaining control laws in the original set.

The first step was to determine a new performance metric and output feedback sensors. During the testing of the previous control laws, strain gauge 8 had the clearest response of the flutter mode and was therefore selected as the primary performance metric and used as the feedback sensor. The trailing-edge outboard accelerometer was used during the closed-loop experiments to gauge the success of control laws at suppressing the overall motion.

Both SISO and MIMO designs were attempted. The SISO designs used a single actuator that was comprised of all 15 individual piezoelectric actuation groups and strain gauge 8 as the sensor and performance metric. The MIMO designs used supergroups A and D and strain gauge 8. These groups were chosen for their effectiveness at controlling the first two modes.

Instead of concentrating on damping at the possible risk of bringing the first two frequencies closer together, the new designs focused on separating the two frequencies to increase the flutter speed with some loss of overall vibration suppression performance. While this objective was not codified in the performance metric, it was used in the decision process of the control design iteration. This effect can be seen in the performance autospectrum for a SISO LQG control law in Fig. 11. Note that this autospectrum is now of strain gauge 8 and not strain gauge 2 as the previous SISO designs were.

Four SISO control laws were tested in all, two LQG designs using varying control authority, a SWLQG, and a classically rationalized design. A MIMO LQG control law was also tested. The most successful of the five control laws was the SISO LQG with the lower control weighting. This control law was able to adequately separate the poles without sacrificing too much damping. Only this SISO control law will be discussed in detail.

F. Redesigned Controller Closed-Loop Testing

Open-loop controller performance evaluation was performed at a dynamic pressure of 50 psf and the control law was deemed stable. The loop was closed and the experimental performance improvement at 50 psf was 2.70 dB (see Fig. 11), which corresponds well to the predicted improvement of 2.92 dB. The dynamic pressure was increased to 75 psf, just under the nominal open-loop flutter dynamic pressure. The vibration

Table 2 Summary of frequencies at zero airspeed for undeployed configuration

	Mode, Hz		
Test	First	Second	Third
First entry	2.51	13.45	17.67
Second entry	2.56	13.75	18.00

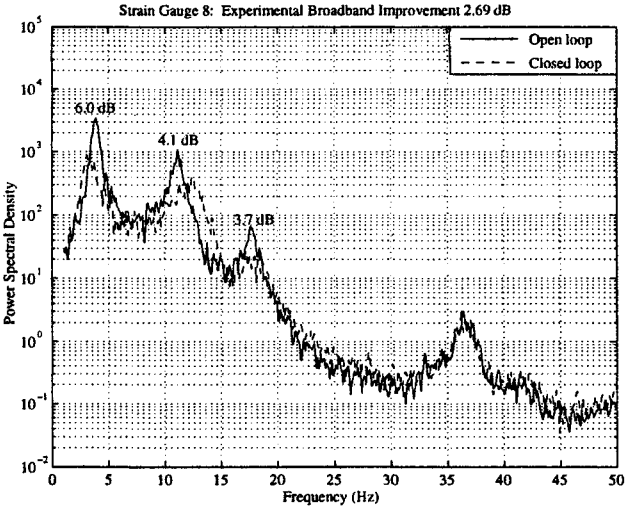

Fig. 11 Experimental open- and closed-loop power spectral densities for LQG control law at 50 psf. Strain gauge 8 is the performance variable.

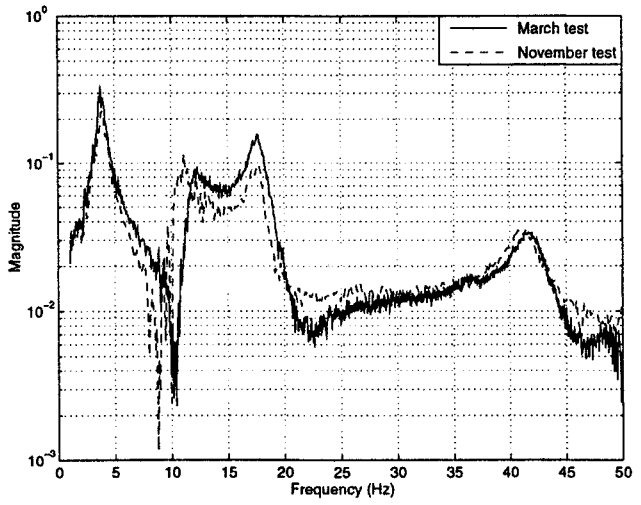

Fig. 10 Comparison of open-loop transfer function data from March and November tests. Input is supergroup 5 and the output is strain gauge 2.

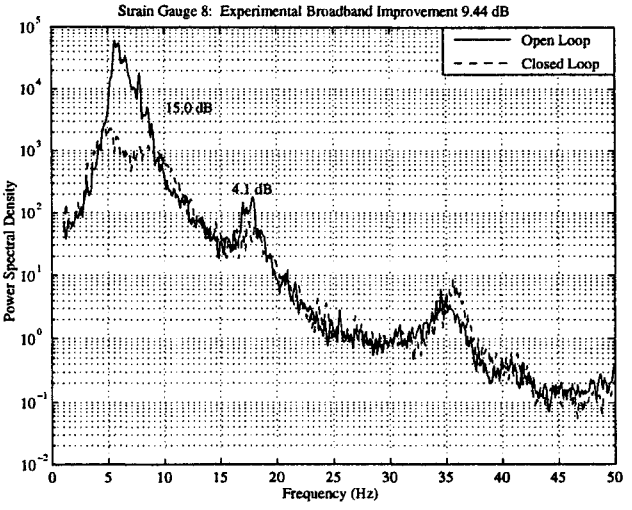

Fig. 12 Experimental open- and closed-loop power spectral densities for LQG control law at 75 psf. Strain gauge 8 is the performance variable.

reduction at 75 psf was significant (see Fig. 12). The modes in the closed-loop plant are still somewhat separated as opposed to the clear single peak in the open-loop plant. Furthermore, at 75 psf, the response of the trailing-edge outboard accelerometer at the flutter frequency was reduced by an order of magnitude with a broadband reduction in power spectral density of 1.1 dB. Not only was the output sensor quieted, but the vibrations of the remainder of the wing were also suppressed.

Because this control law performed well at 75 psf, the closed-loop system was taken above the open-loop flutter point. The tunnel dynamic pressure was increased to 85.5 psf at which the model encountered hard flutter. The approximate total deflection of the test article during this hard flutter was a peak-to-peak tip displacement of 20 in. Visual inspection and frequency rap tests did not indicate any severe damage to the model following the hard flutter.

IV. Analysis of Control Limitations

The closed-loop testing during the second wind-tunnel entry proved to be very successful, with control laws demonstrating significant vibration suppression and flutter suppression. Equally as important as successful vibration and flutter suppression are the reasons why certain control laws did not work and the identifications of performance limiters. There were three major performance limiters: 1) the saturation of the piezoelectrics, 2) the choice of performance metric and output feedback sensor(s), and 3) the high plant variation between the two wind-tunnel entries.

The main limitation on authority was the saturation of the piezoelectrics. Several of the control laws reached the maximum input voltage to the piezoelectrics when the loop was closed. This maximum input voltage was established to prevent actual saturation of the piezoelectrics and utilized the full potential of the piezoelectric actuation range. Even the control laws that did not saturate generally used 80–90% of the maximum voltage.

In addition to the limitation on authority, the near-maximum commanded voltages on the piezoelectrics prevented any effective closed-loop controller performance evaluation. To assess the stability of a control law while closed loop and, more importantly, the stability margins, an additional excitation signal was sent to identify the plant. However, with only 10–20% of the piezoelectric authority available to be used to identify the quieter closed-loop plant, coherent transfer functions were unobtainable. This effectively eliminates adaptive control techniques that require constant identification of the plant.

Two main methods exist to improve this authority: 1) To increase the coverage of the piezoelectrics or 2) to increase the actuation strain of the piezoelectrics. The test article is only partially covered even within the desired region of coverage. If fuller coverage of this region could be obtained, that would certainly increase the authority. Increasing the thickness would not be of much benefit, as the thickness of these actuators was chosen to be near optimal for this test article.[10] The second method is straightforward; if the materials had a higher strain capacity, the effectiveness of these actuators would be greater.[20]

While the authority of the individual patches on the current test article cannot be altered, the authority of the actuation groups used may be improved. The most successful control law (S8) used only one actuator composed of all of the individual patches. Previous studies have shown that to control two modes, two independent actuators are necessary.[13] For aeroelastic control, control of at least the first two modes is desirable. The resulting conclusion is that the piezoelectric actuators could be grouped differently to achieve effective modal control of the first three modes.

Supergroups A–D represent one approach to a multiple actuator grouping. However, these supergroups were chosen based upon the open-loop transfer function data with no air. The individual transfer functions even at zero airspeed were fairly noisy and made the choices somewhat unreliable. In addition, the mode shapes become complex with increasing airspeed, so that effective groupings at 0 psf may not be as effective at 50 psf or higher.

The second performance limitation was the appropriate choice of performance metric and output feedback sensor for vibration and flutter suppression. To completely quiet the wing, a distributed set of sensors would be most appropriate. However, if a limited number of sensors were available, choosing one or two sensors that would most dramatically alter the first two wing mode shapes if their response is suppressed would likely be the most effective. If altered mode shapes are the goal, obtaining a high-fidelity aeroelastic model of the wing is vital to selecting appropriate performance and feedback sensors. The model would need to be particularly accurate for the first three modes for the sensor location choice.

The appropriate choice and use of a MIMO system with a distributed sensor complement is emphasized. A MIMO control law was the only control law able to reduce the response of each of the first three modes, which indicates that a MIMO control law should be most effective for flutter suppression as well. The MIMO control laws were not tested above the nominal design speed of 50 psf because of the test director's concerns for the safety of the model based on visual observation. None of the MIMO control laws were tested in flutter suppression. The two causes are the lack of robustness in the MIMO control laws and the visual judgment of the test engineers. More effective means of robustifying the MIMO control laws are necessary.

The selection and codification of an appropriate performance metric for flutter suppression poses another problem. Ideally, one would like the first two modes to be damped and separated. This is highly unlikely, with one of those objectives generally coming at the expense of the other. Modal damping is a straightforward performance metric to codify for optimal control algorithms. However, as clearly demonstrated during the control law tests, increased modal damping does not indicate that flutter has been postponed. In fact, it is likely that with increased damping, the first two modes are actually closer to coalescence. Frequency separation holds more promise as the correct flutter suppression metric. Unfortunately, the separation of the two frequencies is not an easily codifiable concept for optimal control algorithms.

A third avenue is the alteration of mode shapes to make the first two mode shapes more orthogonal to each other. This is likely the most difficult concept to implement in an optimal control algorithm. In addition to these difficulties, none of these performance metrics provides a guarantee that if achieved, the flutter speed would be increased.

The third important limitation of performance during these closed-loop tests was the high plant variation between the two wind-tunnel entries. This variation is in many ways similar to the variation caused by the changing dynamic pressure. While the quantitative values of the modal frequencies changed, the structure of the transfer function (i.e., pole/zero pattern) did not. If the pole/zero pattern had changed, it would be extraordinarily difficult to design any single control law for the plant. With the structure the same, control laws from optimal design techniques are obtainable; however, the performance on the second mode will necessarily be degraded because of the lack of information about the exact location of the mode.

These changes in the plant indicate that some adaptation would benefit the effectiveness of the control laws. However, as mentioned before, adaptation that requires constant identification using the piezoelectrics is not possible. Therefore, limited adaptation that does not need continual identification of the plant holds promise.

V. Conclusions

This article summarizes the closed-loop testing of the wing test article. Significant vibration and flutter suppression were

demonstrated on a strain-actuated wing test article. Effective control of the first three modes, which include the torsional mode, was achieved through the actuator grouping strategy.

There were several factors that limited performance. These included the authority of the piezoelectric actuators, the choice of actuator/sensor complement, the choice of performance metric, lack of robustness in the MIMO control laws, and the high plant variation. Avenues for future performance improvement were indicated in the preceding section.

Appendix: Performance Prediction

Assume the following system of equations:

$$\begin{aligned} z &= G_{zw}w + G_{zu}u \\ y &= G_{yw}w + G_{yu}u \\ u &= -Ky \end{aligned} \tag{A1}$$

where z is the performance variable, y is the output variable, w is the disturbance, u is the control input, and K is the control law. Then the closed-loop expression is

$$\begin{aligned} z &= \{G_{zw} - G_aG_{yw}\}w \\ G_a &= G_{zu}K[I + G_{yu}K]^{-1} \end{aligned} \tag{A2}$$

The closed-loop power spectral density Φ_{zz} can then be expressed as

$$\begin{aligned} \Phi_{zz} = {} & [G_{zw}(j\omega) - G_a(j\omega)G_{yw}(j\omega)]\Phi_{ww} \\ & \times [G_{zw}(-j\omega) - G_a(-j\omega)G_{yw}(-j\omega)]^T \end{aligned} \tag{A3}$$

This simplifies to the following expression:

$$\begin{aligned} \Phi_{zz} = {} & \Phi_{w_zw_z} - G_a(j\omega)\Phi_{w_yw_z} - \Phi_{w_zw_y}G_a^T(-j\omega) \\ & + G_a(j\omega)\Phi_{w_yw_y}G_a^T(-j\omega) \end{aligned} \tag{A4}$$

where $\Phi_{w_zw_z}$ represents the power spectral density of the disturbance to the performance variables, $\Phi_{w_yw_y}$ represents the power spectral density of the disturbance to the output variables, and $\Phi_{w_yw_z}$ represents the cross-spectral density of the disturbance to the performance and output variables. Note that $w_z = G_{zw}w$ and $w_y = G_{yw}w$.

References

[1]Sandford, M. C., Abel, I., and Gray, D. L., "Development and Demonstration of a Flutter-Suppression System Using Active Controls," NASA TR R-450, Dec. 1975.

[2]Hwang, C., Winther, B. A., Noll, T. E., and Farmer, M. G., "Demonstration of Aircraft Wing/Store Flutter Suppression Systems," AGARD TR R-668, July 1978.

[3]Perry, B. I., Cole, S. R., and Miller, G. D., "Summary of an Active Flexible Wing Program," *Journal of Aircraft*, Vol. 32, No. 1, 1995, pp. 10–15.

[4]Weisshaar, T. A., and Ryan, R. J., "Control of Aeroelastic Instabilities Through Stiffness Cross-Coupling," *Journal of Aircraft*, Vol. 23, No. 2, 1986, pp. 148–155.

[5]Ehlers, S. M., and Weisshaar, T. A., "Adaptive Wing Flexural Control," *Journal of Aircraft*, Vol. 30, No. 4, 1993, pp. 534–540.

[6]Spangler, R. L. J., and Hall, S. R., "Piezoelectric Actuators for Helicopter Rotor Control," *Proceedings of the AIAA/ASME/ASCE/AHS/ASC 31st Structures, Structural Dynamics, and Materials Conference*, AIAA, Washington, DC, 1990, pp. 1589–1599.

[7]Heeg, J., "An Analytical and Experimental Investigation of Flutter Suppression via Piezoelectric Actuation," *Proceedings of the AIAA/ASME/ASCE/AHS/ASC Dynamics Specialists Conference*, AIAA, Washington, DC, 1992, pp. 237–247.

[8]Lazarus, K. B., and Crawley, E. F., "Multivariable High-Authority Control of Plate-Like Active Structures," *Proceedings of the AIAA/ASME/ASCE/AHS/ASC 33rd Structures, Structural Dynamics, and Materials Conference*, AIAA, Washington, DC, 1992, pp. 931–945.

[9]Lazarus, K. B., and Crawley, E. F., "Multivariable Active Lifting Surface Control Using Strain Actuation: Analytical and Experimental Results," *Proceedings of the 3rd International Conference on Adaptive Structures*, Technomic Publishing Co., Lancaster, PA, 1992, pp. 87–101.

[10]Lin, C. Y., and Crawley, E. F., "Design Considerations for a Strain Actuated Adaptive Wing for Aeroelastic Control," *Journal of Intelligent Material Systems and Structures*, Vol. 6, No. 3, 1995, pp. 403–410.

[11]Reich, G. W., Van Schoor, M. C., Lin, C. Y., and Crawley, E. F., "An Active Aeroelastic Wing Model for Vibration and Flutter Suppression," *Proceedings of the AIAA/ASME/ASCE/AHS/ASC 36th Structures, Structural Dynamics, and Materials Conference*, AIAA, Washington, DC, 1995, pp. 314–324.

[12]Heeg, J., McGowan, A., Crawley, E., and Lin, C., "The Piezoelectric Aeroelastic Response Tailoring Investigation: A Status Report," *Proceedings of the SPIE North American Conference on Smart Structures and Materials*, Society of Photo-Optical Instrumentation Engineers, Bellingham, WA, 1995, pp. 2–13.

[13]Lazarus, K. B., Crawley, E. F., and Lin, C. Y., "Fundamental Mechanisms of Aeroelastic Control with Control Surface and Strain Actuation," *Journal of Guidance, Control, and Dynamics*, Vol. 18, No. 1, 1995, pp. 10–17.

[14]Campbell, M. E., and Crawley, E. F., "Classically Rationalized Low Order Robust Structural Controllers," *Proceedings of the AIAA/ASME/ASCE/AHS/ASC 35th Structures, Structural Dynamics, and Materials Conference*, AIAA, Washington, DC, 1994, pp. 1923–1935.

[15]Liu, K., "Identification of Multi-Input and Multi-Output Systems by Observability Range Space Extraction," *Proceedings of the IEEE Conference on Decision and Control*, Inst. of Electrical and Electronics Engineers, Piscataway, NJ, 1992, pp. 915–920.

[16]Jacques, R. N., "On-Line System Identification and Control Design for Flexible Structures." Ph.D. Dissertation, Massachusetts Inst. of Technology, Cambridge, MA, May 1994.

[17]Kwakernaak, H., and Sivan, R., *Linear Optimal Control Systems*, Wiley-Interscience, New York, 1972.

[18]Grocott, S. C. O., How, J. P., and Miller, D. W., "Comparison of Control Techniques for Robust Performance on Uncertain Structural Systems," Massachusetts Inst. of Technology, Space Engineering Research Center, TR 2-94, Cambridge, MA, Jan. 1994.

[19]Pototzky, A. S., Wieseman, C., Hoadley, S. T., and Mukhopadhyay, V., "On-Line Performance Evaluation of Multiloop Digital Control Systems," *Journal of Guidance, Control, and Dynamics*, Vol. 15, No. 4, 1992, pp. 878–883.

[20]Hagood, N., Kindel, R., Ghandi, K., and Gaudenzi, P., "Improving Transverse Actuation of Piezoceramics Using Interdigitated Surface Electrodes," *Proceedings of the Smart Structures and Materials 1993: Smart Structures and Intelligent Systems*, Society of Photo-Optical Instrumentation Engineers, Bellingham, WA, 1993, pp. 341–352.